Calculation of Neutron Response Functions of a NE-213 Scintillator in the Energy Range up to 40 MeV

AUTHOR(S):

SHIN, Kazuo; TOKUMARU, Hiroshi; YOSHIDA, Mitsuo; HYODO, Tomonori

CITATION:

SHIN, Kazuo ...[et al]. Calculation of Neutron Response Functions of a NE-213 Scintillator in the Energy Range up to 40 MeV. Memoirs of the Faculty of Engineering, Kyoto University 1979, 41(2): 116-136

ISSUE DATE:

1979-06-30

URL:

http://hdl.handle.net/2433/281097

Calculation of Neutron Response Functions of a NE-213 Scintillator in the Energy Range up to 40 MeV

By

Kazuo SHIN*, Hiroshi TOKUMARU*, Mitsuo YOSHIDA**
and Tomonori HYODO*

(Received December 25, 1978)

Abstract

A Monte Carlo code was newly made up to calculate the response functions of a 2 inch diam. by 2 inch long NE-213 scintillator for neutrons. The calculated results were compared with the experimental results and fairly good agreement was obtained. Systematic calculations of the NE-213 scintillator response functions were carried out for neutrons incident on the detector parallel to its axis in the energy range up to 40 MeV. Two response matrices, for lower energy up to 17 MeV and for higher energy up to 40 MeV, were made by using the above data. To check the applicability, the low energy matrix was applied to the unfolding of the measured pulse-height spectra. A great improvement was shown in the form of the unfolded spectrum, compared with the spectrum obtained with a response matrix given by Verbinski.

I. Introduction

An organic liquid scintillator NE-213 is widely used in neutron spectroscopy, because it possesses desirable physical characteristics such as good detection efficiency and excellent n-γ discrimination. Accurate knowledge of its neutron response functions and proton light output is necessary in converting pulse height distributions to neutron energy spectra.

Several papers[1)~4)] have been published about the response functions of an NE-213 scintillator for neutrons. They are, however, only for neutrons incident on the detector perpendicular to its axis, and for neutrons whose energies are lower than 20 MeV, excluding the experimental work of Lockwood et al.[4)]. There are large discrepancies among published data[1),2),5),6)] of proton light output which greatly affect the accuracy of the unfolded neutron spectrum as shown by Sasamoto et al.[7)]. These data have the

* Department of Nuclear Engineering
** Present address: Nippon Steel Co., Ltd. 5-3 Tokai-cho, Tokai, Aichi

energy range up to 20 MeV, except for the O5S code library data[2].

In this work, a Monte Carlo code was developed to calculate*) the neutron response functions of a 2 inch diam. by 2 inch long NE-213 scintillator covering the energy range up to 40 MeV, based upon the Monte Carlo codes, CYGNUS[8] and O5S[2]. The calculated results are systematically tabulated in this paper. The calculated response functions were arranged to construct two response matrices for the lower energy range ($E_n \leqq 17$ MeV) and the full energy range ($E_n \leqq 40$ MeV). The two response matrices were already applied to the unfolding of neutron pulse height distributions obtained in the reactor[9] and the accelerator[10),11] shielding experiments, and satisfactorily good results were obtained. In this paper, two examples of unfolded spectra for lower energies are shown. In these spectra, great improvement was shown in the spectral shape, compared with the spectra obtained with Verbinski's data[1].

II. Calculation of Response Function

The response function $R(E_0, h)$ can be written by the following equation, using a light output spectrum $D(E_0, L)$ and a resolution function $G(L, h)$:

$$R(E_0, h)=\int_0^{L_0} D(E_0, L)\ G(L, h)\ dL \tag{1}$$

where $D(E_0, L)dL$ is the probability that a neutron will generate a light yield between L and $L+dL$.

The resolution function $G(L, h)$ can be closely approximated by a Gaussian as follows:

$$G(L, h)=\frac{1}{\sqrt{2\pi}\sigma}\exp\left[-\frac{(L-h)^2}{2\sigma^2}\right]$$
$$\sigma=\sigma_0\sqrt{L} \tag{2}$$

where σ_0 must be determined experimentally.

1 Calculation of D(E_0, L)

i) Monte Carlo Calculation

A Monte Carlo code was developed to calculate the light-output spectrum $D(E_0, L)$ in Eq. (1) for the 2 inch diam. by 2 inch long NE-213 scintillator by modifying the Monte carlo code, CYGNUS[8]. In the calculation, peripheral material components covering the scintillator were all ignored. Composition of the liquid scintillator was determined as shown in Table 1, assuming it to be pure xylene.

Scatterings of neutrons in the scintillator were simulated by random samplings in

*) The calculations of the response functions were made with a FACOM-230-75 computer at the computer center of Kyoto University.

Table 1. Composition of the NE-213 liquid scintillator.

Component	Atomic Dencity (atoms/cm^3)
H	4.99×10^{22}
C	3.99×10^{22}

analogy to the physical process. The Monte Carlo history was terminated when a neutron incident on the detector escaped from it, or was absorbed by (n, p) and (n, α) reactions with carbon, or the neutron energy dropped to a value below cutoff energy, 0.05 MeV, after multiple scatterings in the detector. In the last case, the neutron was assumed to escape from the detector without any more collision. In each history, scintillations generated by secondary charged particles were summed up and the total light output was scored. Contributions from secondary gamma rays which could be generated in neutron reactions were completely ignored in this calculation.

ii) Neutron Reaction Treatments

Most parts of neutron reactions in the detector were handled similarly to the method of the O5S[2] code, so there is only a brief description of the treatments. In this calculation, the following eight types of reactions were considered; H(n, n)H, ^{12}C(n, n)^{12}C, ^{12}C(n, n')^{12}C*, ^{12}C(n, α)^{9}Be, ^{12}C(n, n'3α), ^{12}C(n, p)^{12}B, ^{12}C(n, pn)^{11}B and ^{12}C(n, 2n)^{11}C. Cross section files utilized in the calculation are listed in Table 2. Cross sections of proton recoil and elastic and inelastic scatterings of carbon were taken from the KFK-750[12] file for the energy range below 10 MeV, from the ENDF/B-III[13] file for energies 10–14 MeV, and from the O5S library data for energies higher than 14 MeV.

Angular distributions of scattered neutrons from the hydrogen nucleus were calculated with the second order polynomials in the center of mass (C-M) system, using the data in the O5S code. The sixth-order Legendre expansion was used for an angular distribution of elastically scattered neutrons from carbon in the C-M system. The emission angles of the first neutron from (n, 2n) and the proton from (n, pn) reactions with carbon were sampled from the distributions,

$$p(\theta)=\left(2-\frac{\theta}{\pi}\right)\sin\theta,$$

where θ is the center of mass polar angle. In all other reactions, neutrons were assumed to be emitted isotropically in the C-M system.

An evaporation model was adopted for (n, p), (n, pn) and (n, 2n) reactions in calculating particle energies emerging from these reactions. Lockwood et al.[4] and McNaughton et al.[15] reported that from their experimental data a two-body reaction[4] or a direct quasi-elastic process[15] was recommended rather than the compound process

Table 2. Cross Section Files Whose Data Were Used in the Monte Carlo Calculation.

Nuclide	Reaction Type	File Name	Energy Range (MeV)
Hydrogen	(n, n)	ENDF/B-III[13]	0-14
		O5S Library[2]	14-40
	$\frac{d\sigma}{d\Omega}$	ENDF/B-III	0-14
		O5S Library	14-40
Carbon	σ_{total}	KFK-750[12]	0-10
		ENDF/B-III	10-14
		O5S Library	14-40
	(n, n)	KFK-750	0-10
		ENDF/B-III	10-14
		O5S Library	14-40
	$\frac{d\sigma}{d\Omega}$	O5R Library[14]	0-40
	(n, n')	KFK-750	0-10
		ENDF/B-III	10-14
		O5S Library	14-40
	$\frac{d\sigma}{d\Omega}$	isotropic	0-40
	(n, n' 3α)	O5R Library	0-14
		O5S Library	14-40
	(n, pn)	O5S Library	0-40
	(n, 2n)	O5S Library	0-40
	(n, nα)	O5R Library	0-14
		O5S Library	14-40
	(n, p)	O5S Library	0-40

for the (n, p) and (n, pn) reactions. Bumps due to these reactions, however, were not very prominent in the response functions reported by Lockwood et al., when the incident neutron energy was less than 30 MeV. Errors caused from treating these reactions with a compound model may not be so large in the energy range considered in this paper.

iii) *Energy Deposition of Protons*

The proton range becomes comparable to the detector dimensions as the proton energy becomes higher. When the neutron energy becomes higher, higher energy protons can be generated from the neutron reactions, and larger amounts of wall-end effects can be caused by such high energy protons. To include these effects in the response calculations, the proton transport in the scintillator was treated as follows;

protons were assumed to travel in a straight line for a distance equal to its range. If a crossing of the detector boundary was made by a proton generated with the initial energy E_0, the distance between the crossing point and the end point of its range was computed, and then the proton energy E_b at the boundary was calculated using an energyrange table quoted from the O5S code. The light output ΔL caused by this proton can be described as follows:

$$\Delta L = L(E_0) - L(E_b),$$

where $L(E)$ is the light output caused by the deposition of proton energy E.

2 Light-Output Data

Charged particles such as p, α, Be, B and C, which were generated in the neutron reactions, can produce flashes of light in the scintillator. The light output of the proton is considerably larger than that of other particles, so the proton data are especially important for the response calculations. Large discrepancies, however, were found among the published data for the proton light response. To obtain proton data fit for our scintillator, modification was made on the data reported by Verbinski[1] using our experimental results. This modifying procedure is briefly explained here.

The response measurements were carried out using monocromatic neutrons of the energies 3, 7, 8, 9, 11 and 15 MeV, which were generated from $D(d, n)^3He$ and

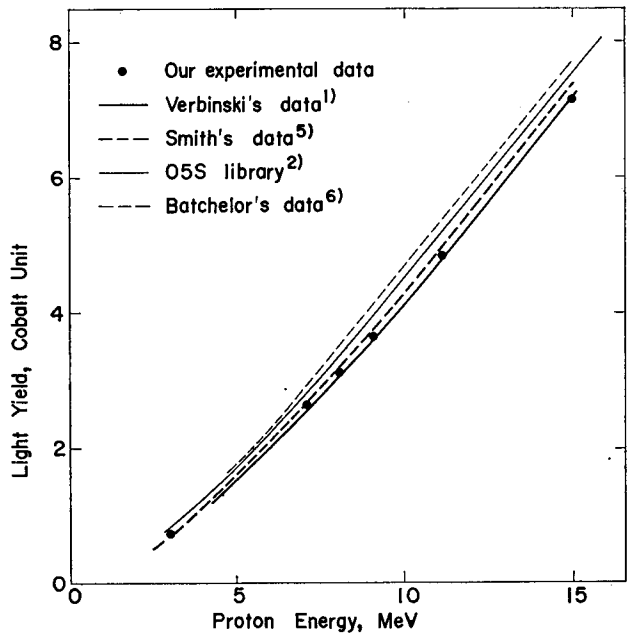

Fig. 1. Comparison of proton light yield data of NE-213 scintillator.

$D(t, n)^4He$ reactions. Deuterons were accelerated by a Cockcroft-Walton accelerator and a tandem-Van de Graff accelerator. The light yields of the maximum energy recoil protons obtained from monoenergy neutrons, were determined from the pulse height of the upper edges in the measured neutron pulse height distributions. The results are shown in Fig. 1 together with the results of others. From this figure, it is clear that our results are very close to Verbinski's[1] curve. The differential curve of his data has two deep depressions at about 5 and 8 MeV. To correct the fault, his data and our results were mixed up and fitted to Birk's formula[1], shown below, by adjusting parameters S and kB with the least square method;

$$L(E)=\int_0^E \frac{S\,dE'}{1+kB\left(\frac{dE'}{dx}\right)}, \qquad (3)$$

(S=0.7974, kB=0.0093)

Table 3. Light Output of the Proton Calculated by Birk's Formula.

Proton Energy (MeV)	Light Yield (Co Unit)	Proton Energy (MeV)	Light Yield (Co Unit)
0.1	0.00945	7.0	2.56298
0.2	0.01898	7.5	2.81832
0.3	0.03024	8.0	3.07878
0.4	0.04329	8.5	3.34386
0.5	0.05809	9.0	3.61313
0.6	0.07444	10.0	4.16278
0.72	0.09609	11.0	4.72574
0.78	0.10767	12.0	5.30079
0.92	0.13652	13.0	5.88656
1.0	0.15409	14.0	6.48189
1.2	0.20119	15.0	7.08588
1.4	0.25242	16.0	7.69778
1.6	0.30742	17.0	8.31684
1.8	0.36585	18.0	8.94240
2.0	0.42738	19.0	9.57398
2.2	0.49176	20.0	10.21115
2.4	0.55883	22.0	11.50060
2.6	0.62836	24.0	12.80796
2.8	0.70016	26.0	14.13102
3.0	0.77406	28.0	15.46792
3.5	0.96694	30.0	16.81714
4.0	1.16988	32.0	18.17746
4.5	1.38216	34.0	19.54770
5.0	1.60349	36.0	20.92703
5.5	1.83296	38.0	22.31458
6.0	2.06974	40.0	23.70972
6.5	2.31326		

where $\frac{dE'}{dx}$ is the specific energy loss[16),17)] of a proton in xylene. The light response of a proton was calculated from this formula in the energy range up to 40 MeV. The calculated results are listed in Table 3.

Light data for α and C ions were obtained from the O5S library data. The C data were also utilized as the data for Be and B ions, because the light responses for these particles were not available.

III. Example of Response Functions

1 Response Function for 15 MeV Neutrons

Response functions were calculated for 15 MeV neutrons incident to a 2 inch diam. by 2 inch long NE-213 scintillator perpendicular and parallel to its axis. The results are shown in Figs. 2 and 3. The response function obtained by the scintillator experimentally for 15 MeV neutrons is shown in Fig. 3. The calculated and measured response functions are compared with the response function obtained by Verbinski in perpendicular incident geometry.

As shown in Fig. 2, our result of perpendicularly incident geometry agrees fairly well with his result. However, in detail, our calculation is a little smaller than his value at the low pulse height, and above this region our value becomes a little larger

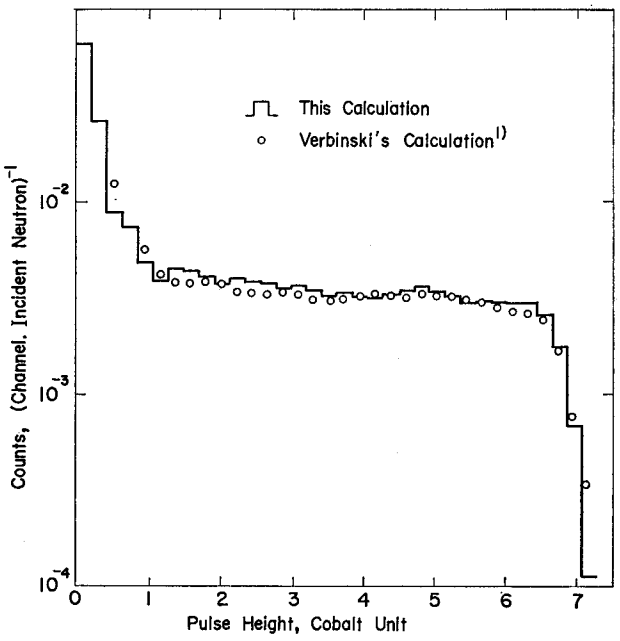

Fig. 2. Comparison of $2''\phi \times 2''$ NE-213 response functions for 15 MeV neutrons obtained in perpendicular incident geometry.

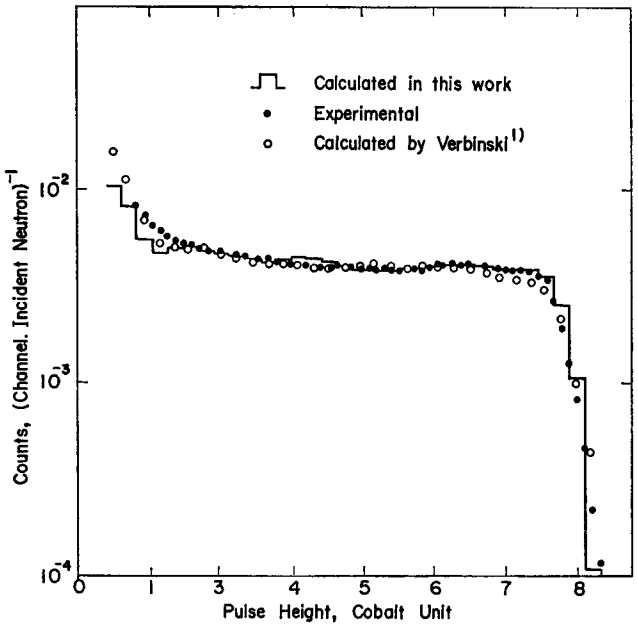

Fig. 3. Comparison of calculated and measured response functions of the 2″ϕ×2″ NE-213 for 15 MeV neutrons in parallel incident geometry.

than his value. The discrepancies may be mainly due to the difference of the cross section data, and partly due to the difference of the light response.

Our results in parallel incident geometry, obtained by caulculation and experiment, are compared with his results and shown in Fig. 3.

All the spectra in the figure agree fairly well with one another. Yet, in detail, some discrepancies can be found. The first one is shown in the vicinity of the upper edge, where his result is a little smaller than the other two spectra. The second is in the low pulse-height region below the 1.5 cobalt unit, where the calculated value of this work is too small. The reason for the latter discrepancy can not be discussed here, because the experimental result may include room-scattered neutrons in this pulse-height region. The former discrepancy is mainly due to the difference of neutron-multiple-scattering effects in the detector, because the direction of the incident neutrons assumed in his calculation was not the same as that of other two spectra. The result of our calculation agrees very well with the experimental one in this region.

2 High Energy Neutrons

Response functions for 27.5 MeV neutrons are shown in Fig. 4. Lockwood's spectrum[4] shown in the figure is a proton energy loss spectrum which was obtained by discriminating proton events from heavier particle events with a pulse-shape-discrimination circuit. The contribution from these heavier particles is included in the calculated

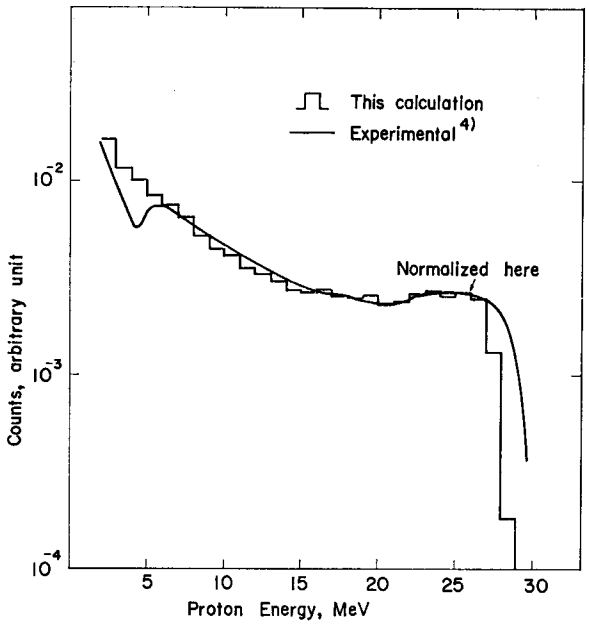

Fig. 4. Comparisor of NE-213 response functions for 27.5 MeV neutrons.

spectrum of this work. But this affects only the first few channels because of their small light outputs compared to the protons.

The two spectra agree very well with each other except for this low energy region. A bump is shown in Lockwood's spectrum near 6 MeV, which is attributed to the $^{12}C(n, p)^{12}B$ reaction in his report. The smoothed shape spectrum was obtained in this calculation, because this reaction was treated with the evaporation model as mentioned in the previous section.

IV. Response Functions for Monoenergetic Neutrons

Calculations of $D(E, L)$ for the 2 inch diam. by 2 inch long NE-213 scintillator were systematically carried out. Incident neutron beams parallel to the detector axis were assumed in the calculation. The calculations were carried out at the step of 0.5 MeV for the incident neutron energies up to 17 MeV, and at the step of 5 MeV for the energies 20–40 MeV.

From the above data, two response matrices were made up, corresponding to the lower energy range up to 17 MeV and to the higher energy range up to 40 MeV. The value of σ_0 in Eq. (2) was fixed at $\sigma_0=0.1$ in the response matrix calculation. The results are shown in Tables 4 and 5. In these tables, the light output L is measured in terms of the absorbed proton energy. The value R_{ji} in i-th row and the j-th column of the tables has the following meaning:

Table 4. Incident Neutron Energies and Response Matrix for Low Energy.

0.0	5.00E−01	1.00E+00	1.50E+00	2.00E+00	2.50E+00	3.00E+00	3.50E+00	4.00E+00	4.50E+00
5.00E+00	5.50E+00	6.00E+00	6.50L+00	7.00E+00	7.50E+00	8.00E+00	8.50E+00	9.00E+00	9.50E+00
1.00E+01	1.05E+01	1.10E+01	1.15E+01	1.20E+01	1.25E+01	1.30E+01	1.35E+01	1.40E+01	1.45E+01
1.50E+01	1.55E+01	1.60E+01	1.65E+01	1.70E+01					

COLM	ROW 1	ROW 2	ROW 3	ROW 4	ROW 5	ROW 6	ROW 7	ROW 8	ROW 9	ROW 10
1	5.566E−01	2.245E−01	1.376E−01	9.353E−02	7.153E−02	5.524E−02	4.477E−02	5.078E−02	4.911E−02	4.099E−02
2	4.489E−02	3.827E−01	1.879E−01	1.106E−01	7.631E−02	5.928E−02	4.873E−02	4.070E−02	3.538E−02	3.154E−02
3	0.0	2.352E−02	2.164E−01	1.531E−01	9.377E−02	6.624E−02	5.211E−02	4.179E−02	3.419E−02	2.907E−02
4	0.0	0.0	1.563E−02	1.263E−01	1.155E−01	7.924E−02	5.737E−02	4.509E−02	3.637E−02	3.030E−02
5	0.0	0.0	0.0	1.249E−02	8.935E−02	8.961E−02	6.972E−02	5.048E−02	4.013E−02	3.133E−02
6	0.0	0.0	0.0	0.0	1.012E−02	6.413E−02	6.504E−02	5.420E−02	4.301E−02	3.361E−02
7	0.0	0.0	0.0	0.0	0.0	8.443E−03	4.818E−02	5.334E−02	4.861E−02	3.835E−02
8	0.0	0.0	0.0	0.0	0.0	3.557E−06	6.868E−03	4.079E−02	4.400E−02	4.193E−02
9	0.0	0.0	0.0	0.0	0.0	0.0	6.763E−06	6.260E−03	3.350E−02	3.627E−02
10	0.0	0.0	0.0	0.0	0.0	0.0	0.0	1.204E−05	5.501E−03	2.922E−02
11	0.0	0.0	0.0	0.0	0.0	0.0	0.0	0.0	1.967E−05	5.265E−03
12	0.0	0.0	0.0	0.0	0.0	0.0	0.0	0.0	0.0	3.050E−05
13	0.0	0.0	0.0	0.0	0.0	0.0	00.	0.0	0.0	0.0

COLM 14 THRU COLM 34 SAME AS ABOVE

Table 4. (cont.)

COLM	ROW 11	ROW 12	ROW 13	ROW 14	ROW 15	ROW 16	ROW 17	ROW 18	ROW 19	ROW 20
1	6.781E−02	6.057E−02	4.748E−02	3.714E−02	5.583E−02	5.498E−02	3.832E−02	3.826E−02	4.014E−02	9.431E−02
2	3.752E−02	3.979E−02	3.497E−02	3.007E−02	4.306E−02	4.491E−02	3.413E−02	3.611E−02	4.008E−02	8.175E−02
3	2.368E−02	2.278E−02	2.287E−02	1.965E−02	1.906E−02	1.641E−02	1.421E−02	1.398E−02	1.384E−02	1.649E−02
4	2.558E−02	2.144E−02	2.027E−02	1.840E−02	1.836E−02	1.720E−02	1.439E−02	1.352E−02	1.134E−02	1.009E−02
5	2.652E−02	2.352E−02	2.040E−02	1.682E−02	1.784E−02	1.535E−02	1.408E−02	1.367E−02	1.223E−02	1.014E−02
6	2.742E−02	2.303E−02	2.023E−02	1.718E−02	1.737E−02	1.457E−02	1.331E−02	1.331E−02	1.195E−02	1.013E−02
7	3.077E−02	2.471E−02	2.047E−02	1.803E−02	1.593E−02	1.399E−02	1.301E−02	1.298E−02	1.165E−02	1.019E−02
8	3.492E−02	2.741E−02	2.183E−02	1.890E−02	1.667E−02	1.378E−02	1.325E−02	1.198E−02	1.148E−02	1.029E−02
9	3.321E−02	2.917E−02	2.345E−02	1.978E−02	1.705E−02	1.457E−02	1.240E−02	1.147E−02	1.109E−02	1.026E−02
10	2.935E−02	2.822E−02	2.507E−02	2.019E−02	1.772E−02	1.584E−02	1.265E−02	1.216E−02	1.031E−02	9.929E−03
11	2.325E−02	2.648E−02	2.481E−02	2.242E−02	2.016E−02	1.677E−02	1.406E−02	1.304E−02	1.088E−02	9.862E−03
12	4.480E−03	2.021E−02	2.260E−02	2.183E−02	1.984E−02	1.766E−02	1.532E−02	1.334E−02	1.116E−02	9.977E−03
13	3.583E−05	3.801E−03	1.793E−02	1.949E−02	1.841E−02	1.724E−02	1.588E−02	1.383E−02	1.127E−02	1.028E−02
14	0.0	3.894E−05	3.634E−03	1.561E−02	1.800E−02	1.640E−02	1.620E−02	1.409E−02	1.167E−02	1.065E−02
15	0.0	0.0	5.701E−05	3.407E−03	1.304E−02	1.571E−02	1.582E−02	1.423E−02	1.210E−02	1.130E−02
16	0.0	0.0	0.0	5.955E−05	2.795E−03	1.225E−02	1.454E−02	1.360E−02	1.224E−02	1.179E−02
17	0.0	0.0	0.0	0.0	4.967E−05	2.837E−03	1.175E−02	1.288E−02	1.202E−02	1.178E−02
18	0.0	0.0	0.0	0.0	0.0	8.105E−05	2.997E−03	9.980E−03	1.172E−02	1.101E−02
19	0.0	0.0	0.0	0.0	0.0	1.025E−07	1.101E−04	2.398E−03	9.013E−03	1.042E−02
20	0.0	0.0	0.0	0.0	0.0	0.0	1.252E−07	9.555E−05	2.261E−03	7.767E−03
21	0.0	0.0	0.0	0.0	0.0	0.0	0.0	1.518E−07	9.331E−05	2.482E−03
22	0.0	0.0	0.0	0.0	0.0	0.0	0.0	0.0	3.491E−07	1.709E−04
23	0.0	0.0	0.0	0.0	0.0	0.0	0.0	0.0	0.0	1.643E−06
24	0.0	0.0	0.0	0.0	0.0	0.0	0.0	0.0	0.0	0.0

COLM 25 THRU COLM 34 SAME AS ABOVE

COLM	ROW 21	ROW 22	ROW 23	ROW 24	ROW 25	ROW 26	ROW 27	ROW 28	ROW 29	ROW 30
1	9.353E−02	1.065E−01	8.157E−02	8.680E−02	8.767E−02	8.782E−02	8.263E−02	7.128E−02	7.207E−02	7.336E−02
2	8.755E−02	1.065E−01	8.157E−02	8.680E−02	8.767E−02	8.782E−02	8.263E−02	7.128E−02	7.207E−02	7.336E−02
3	1.802E−02	2.021E−02	3.459E−02	3.752E−02	3.847E−02	4.018E−02	4.246E−02	4.630E−02	4.999E−02	5.390E−02
4	1.022E−02	1.139E−02	1.811E−02	1.892E−02	1.774E−02	1.567E−02	1.471E−02	2.298E−02	2.212E−02	2.022E−02
5	9.301E−03	8.608E−03	9.690E−03	9.630E−03	9.858E−03	1.067E−02	1.032E−02	1.055E−02	1.122E−02	1.192E−02
6	9.330E−03	8.491E−03	8.048E−03	7.560E−03	7.290E−03	7.049E−03	7.891E−03	8.125E−03	8.286E−03	8.416E−03
7	9.422E−03	8.795E−03	8.023E−03	7.268E−03	6.644E−03	6.321E−03	6.536E−03	6.466E−03	6.543E−03	6.653E−03
8	9.426E−03	8.873E−03	7.959E−03	7.206E−03	6.612E−03	6.244E−03	5.963E−03	5.626E−03	5.540E−03	5.435E−03
9	9.236E−03	8.906E−03	8.000E−03	7.161E−03	6.700E−03	6.209E−03	5.871E−03	5.335E−03	5.185E−03	5.007E−03
10	9.085E−03	8.588E−03	7.861E−03	7.232E−03	6.793E−03	6.232E−03	5.844E−03	5.333E−03	5.192E−03	4.918E−03
11	8.964E−03	8.174E−03	7.783E−03	7.328E−03	6.865E−03	6.229E−03	5.901E−03	5.376E−03	5.162E−03	4.902E−03
12	8.836E−03	8.127E−03	7.815E−03	7.374E−03	6.835E−03	6.323E−03	5.911E−03	5.469E−03	5.154E−03	4.960E−03
13	8.952E−03	8.333E−03	7.925E−03	7.305E−03	6.674E−03	6.510E−03	5.871E−03	5.571E−03	5.242E−03	4.955E−03
14	9.241E−03	8.434E−03	8.035E−03	7.142E−03	6.639E−03	6.486E−03	5.900E−03	5.569E−03	5.198E−03	4.916E−03
15	9.619E−03	8.787E−03	8.176E−03	7.157E−03	6.747E−03	6.353E−03	5.968E−03	5.561E−03	5.186E−03	4.883E−03
16	1.008E−02	9.153E−03	8.291E−03	7.279E−03	6.690E−03	6.217E−03	5.870E−03	5.475E−03	5.181E−03	4.811E−03
17	1.059E−02	9.453E−03	8.553E−03	7.512E−03	6.781E−03	6.290E−03	5.823E−03	5.499E−03	5.154E−03	4.809E−03
18	1.044E−02	9.621E−03	8.768E−03	7.662E−03	6.933E−03	6.418E−03	5.772E−03	5.453E−03	5.115E−03	4.813E−03
19	9.842E−03	9.629E−03	8.879E−03	7.943E−03	7.194E−03	6.558E−03	5.855E−03	5.485E−03	5.144E−03	4.909E−03
20	9.039E−03	9.161E−03	8.555E−03	8.194E−03	7.442E−03	6.739E−03	6.122E−03	5.519E−03	5.135E−03	4.951E−03
21	6.947E−03	8.565E−03	8.328E−03	8.017E−03	7.529E−03	6.989E−03	6.499E−03	5.706E−03	5.229E−03	4.968E−03
22	2.175E−03	6.415E−03	7.875E−03	7.462E−03	7.259E−03	6.939E−03	6.668E−03	5.928E−03	5.311E−03	4.991E−03
23	1.977E−04	2.033E−03	6.078E−03	7.008E−03	7.057E−03	6.661E−03	6.580E−03	6.195E−03	5.506E−03	5.198E−03
24	3.805E−06	2.077E−04	1.912E−03	5.412E−03	6.606E−03	6.406E−03	6.267E−03	6.071E−03	5.634E−03	5.327E−03
25	0.0	4.733E−06	2.275E−04	1.734E−03	5.063E−03	6.024E−03	5.979E−03	5.828E−03	5.566E−03	5.374E−03
26	0.0	0.0	5.181E−06	2.368E−04	1.657E−03	4.657E−03	5.633E−03	5.704E−03	5.473E−03	5.337E−03
27	0.0	0.0	0.0	4.780E−06	2.395E−04	1.522E−03	4.424E−03	5.410E−03	5.411E−03	5.169E−03
28	0.0	0.0	0.0	1.420E−08	4.182E−06	2.292E−04	1.495E−03	4.178E−03	5.126E−03	4.995E−03
29	0.0	0.0	0.0	0.0	4.685E−08	3.304E−06	2.379E−04	1.426E−03	3.912E−03	4.732E−03
30	0.0	0.0	0.0	0.0	0.0	0.0	7.930E−06	2.294E−04	1.319E−03	3.628E−03
31	0.0	0.0	0.0	0.0	0.0	0.0	0.0	1.048E−05	2.115E−04	1.262E−03
32	0.0	0.0	0.0	0.0	0.0	0.0	0.0	0.0	1.091E−05	2.004E−04
33	0.0	0.0	0.0	0.0	0.0	0.0	0.0	0.0	0.0	1.129E−05
34	0.0	0.0	0.0	0.0	0.0	0.0	0.0	0.0	0.0	9.312E−08

Table 4. (cont.)

COLM	ROW 31	ROW 32	ROW 33	ROW 34
1	7.385E−02	7.468E−02	7.133E−02	6.852E−02
2	7.385E−02	7.468E−02	7.133E−02	6.852E−02
3	5.760E−02	6.236E−02	6.370E−02	6.513E−02
4	1.750E−02	1.627E−02	1.518E−02	1.410E−02
5	1.205E−02	1.231E−03	1.227E−02	1.225E−02
6	8.455E−03	8.445E−03	7.805E−03	7.359E−03
7	6.594E−03	6.122E−03	5.966E−03	6.239E−03
8	5.649E−03	5.570E−03	5.384E−03	5.536E−03
9	5.008E−03	5.049E−03	4.956E−03	4.955E−03
10	4.671E−03	4.649E−03	4.618E−03	4.580E−03
11	4.537E−03	4.467E−03	4.254E−03	4.266E−03
12	4.504E−03	4.404E−03	4.118E−03	4.093E−03
13	4.552E−03	4.354E−03	4.101E−03	4.048E−03
14	4.596E−03	4.242E−03	4.083E−03	4.031E−03
15	4.596E−03	4.283E−03	4.097E−03	3.966E−03
16	4.577E−03	4.265E−03	4.095E−03	3.957E−03
17	4.545E−03	4.290E−03	4.097E−03	3.896E−03
18	4.504E−03	4.243E−03	4.117E−03	3.797E−03
19	4.509E−03	4.219E−03	4.059E−03	3.829E−03
20	4.488E−03	4.195E−03	3.958E−03	3.779E−03
21	4.532E−03	4.228E−03	3.987E−03	3.809E−03
22	4.587E−03	4.211E−03	4.046E−03	3.824E−03
23	4.695E−03	4.271E−03	4.097E−03	3.915E−03
24	4.789E−03	4.346E−03	4.136E−03	3.900E−03
25	4.909E−03	4.418E−03	4.202E−03	3.855E−03
26	5.030E−03	4.597E−03	4.330E−03	3.933E−03
27	4.993E−03	4.682E−03	4.444E−03	4.073E−03
28	4.784E−03	4.550E−03	4.435E−03	4.182E−03
29	4.566E−03	4.424E−03	4.333E−03	4.217E−03
30	4.314E−03	4.344E−03	4.207E−03	4.177E−03
31	3.376E−03	4.140E−03	4.128E−03	4.127E−03
32	1.180E−03	3.149E−03	3.935E−03	4.068E−03
33	1.907E−04	1.118E−03	2.982E−03	3.814E−03
34	1.152E−05	1.826E−04	1.079E−03	2.837E−03

Table 5. Incident Neutron Energies and Response Matrix for High Energy Neutrons.

0.0	1.0E+00	2.0E+00	3.0E+00	4.0E+00	5.0E+00	6.0E+00	7.0E+00	8.0E+00	9.0E+00
1.0E+01	1.1E+01	1.2E+01	1.3E+01	1.4E+01	1.5E+01	1.6E+01	1.7E+01	1.8E+01	1.9E+01
2.0E+01	2.1E+01	2.2E+01	2.3E+01	2.4E+01	2.5E+01	2.6E+01	2.7E+01	2.8E+01	2.9E+01
3.0E+01	3.1E+01	3.2E+01	3.3E+01	3.4E+01	3.5E+01	3.6E+01	3.7E+01	3.8E+01	3.9E+01
4.0E+01									

COLM	ROW 1	ROW 2	ROW 3	ROW 4	ROW 5	ROW 6	ROW 7	ROW 8	ROW 9	ROW 10
1	8.864E−01	4.775E−01	3.021E−01	2.852E−01	2.274E−01	1.924E−01	1.790E−01	2.156E−01	1.790E−01	1.894E−01
2	0.0	2.367E−01	1.825E−01	1.184E−01	7.342E−02	5.006E−02	3.645E−02	3.423E−02	2.300E−02	2.131E−02
3	0.0	0.0	1.179E−01	1.525E−01	8.097E−02	5.311E−02	3.975E−02	3.906E−02	2.562E−02	2.187E−02
4	0.0	0.0	0.0	8.182E−02	1.012E−01	5.784E−02	4.086E−02	3.856E−02	2.603E−02	2.258E−02
5	0.0	0.0	0.0	0.0	4.780E−02	6.724E−02	4.467E−02	3.969E−02	2.613E−02	2.236E−02
6	0.0	0.0	0.0	0.0	0.0	3.022E−02	4.770E−02	4.427E−02	2.707E−02	2.222E−02
7	0.0	0.0	0.0	0.0	0.0	5.153E−04	2.195E−02	4.430E−02	3.008E−02	2.407E−02
8	0.0	0.0	0.0	0.0	0.0	0.0	4.902E−04	2.031E−02	2.849E−02	2.600E−02
9	0.0	0.0	0.0	0.0	0.0	0.0	0.0	5.767E−04	1.312E−02	2.374E−02
10	0.0	0.0	0.0	0.0	0.0	0.0	0.0	0.0	4.577E−04	1.112E−02
11	0.0	0.0	0.0	0.0	0.0	0.0	0.0	0.0	0.0	4.644E−04
12	0.0	0.0	0.0	0.0	0.0	0.0	0.0	0.0	0.0	0.0

COLM 13 THRU COLM 40 SAME AS ABOVE

Table 5. (cont.)

COLM	ROW 11	ROW 12	ROW 13	ROW 14	ROW 15	ROW 16	ROW 17	ROW 18	ROW 19	ROW 20
1	1.859E−01	1.902E−01	1.961E−01	1.874E−01	1.825E−01	1.870E−01	1.788E−01	1.609E−01	1.536E−01	1.433E−01
2	2.281E−02	2.638E−02	3.126E−02	3.447E−02	3.673E−02	3.908E−02	4.341E−02	5.112E−02	6.008E−02	6.492E−02
3	1.795E−02	1.650E−02	1.627E−02	1.521E−02	1.625E−02	1.836E−02	1.918E−02	1.844E−02	1.829E−02	1.896E−02
4	1.853E−02	1.567E−02	1.400E−02	1.210E−02	1.123E−02	1.190E−02	1.238E−02	1.244E−02	1.311E−02	1.319E−02
5	1.835E−02	1.601E−02	1.399E−02	1.150E−02	1.017E−02	1.008E−02	9.944E−03	1.027E−02	1.132E−02	1.190E−02
6	1.807E−02	1.580E−02	1.391E−02	1.168E−02	9.997E−03	9.182E−03	9.065E−03	9.221E−03	9.909E−03	1.029E−02
7	1.888E−02	1.574E−02	1.392E−02	1.157E−02	9.784E−03	9.112E−03	8.105E−03	7.495E−03	7.831E−03	8.673E−03
8	1.960E−02	1.642E−02	1.411E−02	1.127E−02	9.986E−03	8.792E−03	7.728E−03	6.701E−03	6.312E−03	6.095E−03
9	2.149E−02	1.716E−02	1.423E−02	1.194E−02	9.684E−03	8.656E−03	8.011E−03	6.617E−03	6.075E−03	5.598E−03
10	1.895E−02	1.851E−02	1.531E−02	1.178E−02	9.772E−03	9.160E−03	7.548E−03	6.600E−03	6.311E−03	5.463E−03
11	9.105E−03	1.611E−02	1.636E−02	1.271E−02	1.017E−02	8.540E−03	7.767E−03	6.724E−03	5.911E−03	5.511E−03
12	4.425E−04	7.894E−03	1.414E−02	1.350E−02	1.104E−02	9.487E−03	7.604E−03	6.593E−03	6.202E−03	5.451E−03
13	0.0	4.371E−04	6.996E−03	1.171E−02	1.143E−02	1.004E−02	8.243E−03	6.578E−03	5.865E−03	5.370E−03
14	0.0	0.0	4.336E−04	5.814E−03	9.979E−03	1.031E−02	8.942E−03	7.020E−03	5.963E−03	5.341E−03
15	0.0	0.0	0.0	3.982E−04	4.979E−03	8.918E−03	8.997E−03	7.827E−03	6.456E−03	5.377E−03
16	0.0	0.0	0.0	0.0	3.724E−04	4.486E−03	7.618E−03	7.614E−03	7.184E−03	5.758E−03
17	0.0	0.0	0.0	0.0	0.0	3.634E−04	3.868E−03	6.386E−03	6.858E−03	6.452E−03
18	0.0	0.0	0.0	0.0	0.0	0.0	3.370E−04	3.252E−03	5.727E−03	5.996E−03
19	0.0	0.0	0.0	0.0	0.0	0.0	0.0	3.026E−04	2.906E−03	5.095E−03
20	0.0	0.0	0.0	0.0	0.0	0.0	0.0	0.0	2.863E−04	2.551E−03
21	0.0	0.0	0.0	0.0	0.0	0.0	0.0	0.0	0.0	2.638E−04
22	0.0	0.0	0.0	0.0	0.0	0.0	0.0	0.0	0.0	0.0

COLM 23 THRU COLM 40 SAME AS ABOVE

COLM	ROW 21	ROW 22	ROW 23	ROW 24	ROW 25	ROW 26	ROW 27	ROW 28	ROW 29	ROW 30
1	1.337E−01	1.257E−01	1.183E−01	1.113E−01	1.052E−01	9.994E−02	9.497E−02	9.007E−02	8.559E−02	8.153E−02
2	6.882E−02	7.280E−02	7.629E−02	7.935E−02	8.230E−02	8.534E−02	8.807E−02	9.025E−02	9.223E−02	9.410E−02
3	1.958E−02	1.977E−02	1.947E−02	1.895E−02	1.833E−02	1.773E−02	1.715E−02	1.658E−02	1.612E−02	1.550E−02
4	1.301E−02	1.319E−02	1.340E−02	1.329E−02	1.309E−02	1.281E−02	1.238E−02	1.185E−02	1.130E−02	1.088E−02
5	1.207E−02	1.192E−02	1.163E−02	1.152E−02	1.145E−02	1.103E−02	1.057E−02	1.015E−02	9.823E−03	9.672E−03
6	1.055E−02	1.062E−02	1.064E−02	1.024E−02	9.762E−03	9.523E−03	9.062E−03	8.527E−03	8.018E−03	7.626E−03
7	9.255E−03	9.294E−03	9.150E−03	9.041E−03	8.894E−03	8.461E−03	8.077E−03	7.585E−03	6.995E−03	6.450E−03
8	6.312E−03	6.867E−03	7.158E−03	7.322E−03	7.175E−03	7.254E−03	6.896E−03	6.586E−03	6.277E−03	5.881E−03
9	5.328E−03	5.373E−03	5.576E−03	5.658E−03	5.752E−03	5.502E−03	5.498E−03	5.322E−03	5.181E−03	5.004E−03
10	5.025E−03	4.901E−03	4.963E−03	5.106E−03	5.228E−03	5.068E−03	4.743E−03	4.504E−03	4.228E−03	4.074E−03
11	5.126E−03	4.680E−03	4.475E−03	4.398E−03	4.462E−03	4.594E−03	4.533E−03	4.162E−03	3.817E−03	3.584E−03
12	4.811E−03	4.536E−03	4.326E−03	4.139E−03	4.040E−03	3.912E−03	3.692E−03	3.597E−03	3.552E−03	3.426E−03
13	4.891E−03	4.500E−03	4.064E−03	3.769E−03	3.683E−03	3.632E−03	3.524E−03	3.369E−03	3.113E−03	2.806E−03
14	4.867E−03	4.434E−03	3.991E−03	3.775E−03	3.460E−03	3.204E−03	3.156E−03	3.068E−03	2.976E−03	2.885E−03
15	4.698E−03	4.383E−03	3.996E−03	3.691E−03	3.382E−03	3.212E−03	2.932E−03	2.764E−03	2.688E−03	2.582E−03
16	4.828E−03	4.236E−03	4.052E−03	3.636E−03	3.360E−03	3.148E−03	2.907E−03	2.700E−03	2.492E−03	2.402E−03
17	5.167E−03	4.379E−03	3.832E−03	3.689E−03	3.365E−03	3.055E−03	2.900E−03	2.746E−03	2.478E−03	2.293E−03
18	5.754E−03	4.698E−03	3.984E−03	3.426E−03	3.373E−03	3.128E−03	2.771E−03	2.575E−03	2.533E−03	2.383E−03
19	5.219E−03	5.143E−03	4.334E−03	3.615E−03	3.087E−03	2.980E−03	2.890E−03	2.545E−03	2.335E−03	2.244E−03
20	4.563E−03	4.578E−03	4.542E−03	3.948E−03	3.320E−03	2.841E−03	2.834E−03	2.617E−03	2.377E−03	2.113E−03
21	2.262E−03	4.122E−03	4.052E−03	4.030E−03	3.575E−03	3.099E−03	2.606E−03	2.328E−03	2.310E−03	2.214E−03
22	2.445E−04	2.049E−03	3.722E−03	3.640E−03	3.595E−03	3.253E−03	2.884E−03	2.413E−03	2.106E−03	2.113E−03
23	0.0	2.311E−04	1.867E−03	3.360E−03	3.336E−03	3.199E−03	2.982E−03	2.690E−03	2.238E−03	1.937E−03
24	0.0	0.0	2.196E−04	1.711E−03	3.049E−03	3.103E−03	2.873E−03	2.737E−03	2.542E−03	2.068E−03
25	0.0	0.0	0.0	2.099E−04	1.580E−03	2.826E−03	2.875E−03	2.594E−03	2.511E−03	2.398E−03
26	0.0	0.0	0.0	0.0	2.023E−04	1.480E−03	2.651E−03	2.644E−03	2.369E−03	2.284E−03
27	0.0	0.0	0.0	0.0	0.0	1.966E−04	1.392E−03	2.486E−03	2.423E−03	2.189E−03
28	0.0	0.0	0.0	0.0	0.0	5.889E−07	1.919E−04	1.309E−03	2.334E−03	2.216E−03
29	0.0	0.0	0.0	0.0	0.0	0.0	6.900E−07	1.856E−04	1.231E−03	2.185E−03
30	0.0	0.0	0.0	0.0	0.0	0.0	0.0	7.953E−07	1.793E−04	1.157E−03
31	0.0	0.0	0.0	0.0	0.0	0.0	0.0	0.0	9.038E−07	1.728E−04
32	0.0	0.0	0.0	0.0	0.0	0.0	0.0	0.0	0.0	1.013E−06
33	0.0	0.0	0.0	0.0	0.0	0.0	0.0	0.0	0.0	0.0

COLM 34 THRU COLM 40 SAME AS ABOVE

Table 5. (cont.)

COLM	ROW 31	ROW 32	ROW 33	ROW 34	ROW 35	ROW 36	ROW 37	ROW 38	ROW 39	ROW 40
1	7.766E−02	7.393E−02	7.038E−02	6.701E−02	6.382E−02	6.074E−02	5.780E−02	5.505E−02	5.249E−02	5.013E−02
2	9.563E−02	9.677E−02	9.761E−02	9.463E−02	9.014E−02	8.582E−02	8.168E−02	7.780E−02	7.420E−02	7.089E−02
3	1.470E−02	1.402E−02	1.344E−02	1.647E−02	2.082E−02	2.474E−02	2.825E−02	3.137E−02	3.416E−02	3.665E−02
4	1.075E−02	1.069E−02	1.068E−02	1.073E−02	1.083E−02	1.100E−02	1.120E−02	1.141E−02	1.159E−02	1.175E−02
5	9.279E−03	8.861E−03	8.472E−03	8.129E−03	7.844E−03	7.658E−03	7.570E−03	7.468E−03	7.207E−03	6.949E−03
6	7.442E−03	7.202E−03	6.985E−03	6.779E−03	6.577E−03	6.393E−03	6.121E−03	5.797E−03	5.700E−03	5.644E−03
7	6.132E−03	5.905E−03	5.670E−03	5.446E−03	5.235E−03	5.067E−03	4.926E−03	4.884E−03	4.818E−03	4.730E−03
8	5.555E−03	5.340E−03	5.024E−03	4.755E−03	4.536E−03	4.378E−03	4.284E−03	4.204E−03	4.122E−03	4.031E−03
9	4.709E−03	4.501E−03	4.401E−03	4.214E−03	4.037E−03	3.872E−03	3.738E−03	3.626E−03	3.545E−03	3.483E−03
10	3.949E−03	3.735E−03	3.581E−03	3.454E−03	3.360E−03	3.308E−03	3.266E−03	3.158E−03	3.044E−03	2.923E−03
11	3.499E−03	3.365E−03	3.165E−03	2.998E−03	2.817E−03	2.649E−03	2.601E−03	2.610E−03	2.608E−03	2.590E−03
12	3.103E−03	2.983E−03	2.969E−03	2.980E−03	2.819E−03	2.570E−03	2.338E−03	2.230E−03	2.155E−03	2.108E−03
13	2.792E−03	2.842E−03	2.722E−03	2.521E−03	2.485E−03	2.489E−03	2.438E−03	2.239E−03	2.033E−03	1.868E−03
14	2.698E−03	2.461E−03	2.377E−03	2.408E−03	2.387E−03	2.236E−03	2.076E−03	2.012E−03	1.962E−03	1.885E−03
15	2.524E−03	2.482E−03	2.344E−03	2.206E−03	2.116E−03	2.105E−03	2.050E−03	1.967E−03	1.831E−03	1.715E−03
16	2.277E−03	2.152E−03	2.147E−03	2.140E−03	2.038E−03	1.970E−03	1.917E−03	1.838E−03	1.777E−03	1.697E−03
17	2.201E−03	2.080E−03	1.877E−03	1.812E−03	1.842E−03	1.850E−03	1.823E−03	1.803E−03	1.755E−03	1.650E−03
18	2.153E−03	2.060E−03	2.031E−03	1.824E−03	1.580E−03	1.595E−03	1.663E−03	1.645E−03	1.621E−03	1.626E−03
19	2.206E−03	2.039E−03	1.937E−03	1.911E−03	1.877E−03	1.632E−03	1.441E−03	1.506E−03	1.562E−03	1.498E−03
20	2.005E−03	1.953E−03	1.865E−03	1.771E−03	1.767E−03	1.730E−03	1.659E−03	1.481E−03	1.369E−03	1.433E−03
21	1.999E−03	1.842E−03	1.733E−03	1.656E−03	1.596E−03	1.597E−03	1.556E−03	1.471E−03	1.440E−03	1.355E−03
22	2.024E−03	1.934E−03	1.777E−03	1.589E−03	1.506E−03	1.429E−03	1.447E−03	1.462E−03	1.334E−03	1.257E−03
23	1.911E−03	1.846E−03	1.822E−03	1.758E−03	1.559E−03	1.400E−03	1.312E−03	1.309E−03	1.343E−03	1.308E−03
24	1.861E−03	1.734E−03	1.700E−03	1.684E−03	1.661E−03	1.550E−03	1.357E−03	1.228E−03	1.191E−03	1.232E−03
25	1.981E−03	1.790E−03	1.620E−03	1.567E−03	1.544E−03	1.511E−03	1.453E−03	1.321E−03	1.215E−03	1.075E−03
26	2.206E−03	1.916E−03	1.720E−03	1.561E−03	1.458E−03	1.413E−03	1.380E−03	1.309E−03	1.238E−03	1.189E−03
27	2.060E−03	2.004E−03	1.821E−03	1.656E−03	1.498E−03	1.408E−03	1.308E−03	1.288E−03	1.181E−03	1.124E−03
28	1.999E−03	1.871E−03	1.829E−03	1.686E−03	1.598E−03	1.416E−03	1.379E−03	1.231E−03	1.198E−03	1.106E−03
29	1.995E−03	1.790E−03	1.698E−03	1.683E−03	1.534E−03	1.467E−03	1.321E−03	1.303E−03	1.208E−03	1.109E−03
30	2.003E−03	1.775E−03	1.591E−03	1.542E−03	1.564E−03	1.395E−03	1.283E−03	1.210E−03	1.200E−03	1.186E−03
31	1.072E−03	1.795E−03	1.581E−03	1.409E−03	1.395E−03	1.464E−03	1.265E−03	1.127E−03	1.080E−03	1.084E−03
32	1.644E−04	9.777E−04	1.602E−03	1.414E−03	1.257E−03	1.270E−03	1.354E−03	1.177E−03	1.006E−03	9.445E−04
33	1.114E−06	1.546E−04	8.876E−04	1.427E−03	1.277E−03	1.162E−03	1.195E−03	1.251E−03	1.112E−03	9.282E−04
34	0.0	1.198E−06	1.446E−04	8.037E−04	1.273E−03	1.181E−03	1.120E−03	1.132E−03	1.156E−03	1.051E−03
35	0.0	0.0	1.273E−06	1.350E−04	7.276E−04	1.147E−03	1.116E−03	1.090E−03	1.080E−03	1.074E−03
36	0.0	0.0	0.0	1.340E−06	1.260E−04	6.615E−04	1.044E−03	1.056E−03	1.067E−03	1.033E−03
37	0.0	0.0	0.0	0.0	1.400E−06	1.178E−04	6.052E−04	9.579E−04	1.000E−03	1.041E−03
38	0.0	0.0	0.0	0.0	0.0	1.457E−06	1.106E−04	5.566E−04	8.853E−04	9.471E−04
39	0.0	0.0	0.0	0.0	0.0	0.0	1.515E−06	1.042E−04	5.152E−04	8.251E−04
40	0.0	0.0	0.0	0.0	0.0	0.0	0.0	1.571E−06	9.856E−05	4.805E−04

$$R_{ji}=\int_{E_{j-1}}^{E_j} R(E_i, h)dh, \quad (E_0=0 \text{ MeV}) \tag{4}$$

where E_i is the incident neutron energy.

The estimated statistical errors in the values of Tables 4 and 5 are about 5% and 10% at maximum, respectively.

V. Application of Response Matrix

In this section the low energy response matrix, shown in Table 4, is applied to the unfolding of the measured pulse-height spectra to check its applicability. The Ferdo[17] code was used in the unfolding.

1 Continuous Spectrum

Shielding experiments[9] were performed at the fast column of the fast neutron source reactor "YAYOI" of University of Tokyo. In Fig. 5, the source spectrum of this experiment, measured in the neutron beam from the column, is compared with the

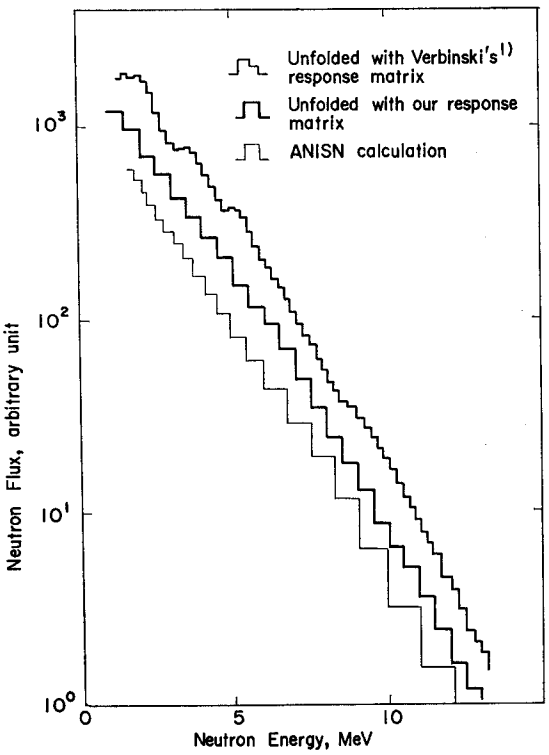

Fig. 5. Comparison of unfolded spectra with ANISN calculation for the leakage neutrons from "YAYOI." reactor.

ANISN[19] calculation for the leakage neutron spectrum from the blanket. The unfolding of the measured pulse-height spectrum was done using the following two data sets: One is a response matrix constructed from Verbinski's data[1] combined with his light outputs[1], and the other is the matrix of this work with the light data shown in Table 2. From the figure, the result obtained with the response matrix of this work agrees very well in the spectral shape with the calculated result. Appreciably large fluctuations are seen near 3.5, 5.0 and 9.0 MeV in the spectrum unfolded with Verbinski's response matrix. This abnormal shape can be explained clearly by the depression in the differential curve of Verbinski's light output data for a proton.

2 Monocromatic Neutrons

The measured pulse height distribution which was already shown in Fig. 3 was unfolded with the same data sets, mentioned in the above section, to show the improvement in the spectral shape by the response data of this work. The results are shown in Fig. 6. The amount of room-scattered neutrons seems to be very small, except for the low energy region, compared with the amount of direct components from the source. Therefore, the spectrum should be a detector-resolution function at energies near 15 MeV. Both unfolded spectra become negative at the energy just below the 15-MeV

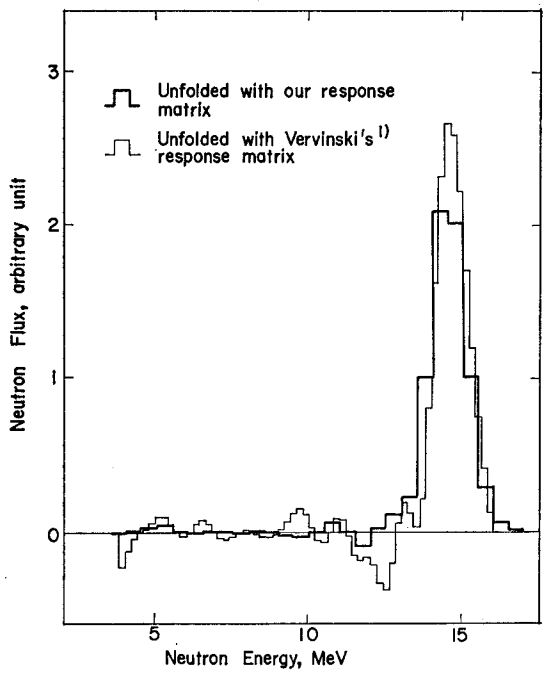

Fig. 6. Comparison of neutron spectra for 15 MeV neutrons obtained with two different response data.

peak and oscillate in the lower energy region. However, the spectral shape of this work is improved very much, compared with that obtained by Verbinski's response functions.

VI. Conclusion

Calculations of the neutron response functions of the 2 inch diam. by 2 inch long NE-213 scintillator were performed systematically, covering the energy range up to 40 MeV. The new proton light output data which agreed with our experimental data in the lower energy region were obtained up to 40 MeV using Birk's formula. The calculated pulse height spectra were compared with experimental ones and good agreement was obtained. Response matrices were calculated and one of them was applied to the unfolding of two neutron spectra to get satisfactory improvements in the spectral shapes, in comparison with Verbinski's response matrix.

Acknowledgement

The authors wish to thank Dr. T. Nakamura and Dr. H. Hirayama for their useful suggestions on the Monte Carlo calculation. The authors are grateful to Messers. S. Shiroya, S. Ban and T. Nishibe for their co-operation in the experiment on this study. The authors express their gratitude to Mr. M. Fujii for his helpful assistance with this paper.

References

1) V. V. Verbinski et al, "The Response of Some Organic Scintillators to Fast Neutrons", ANS-SD-2, 189 (1964).
2) R. E. Textor and V. V. Verbinski, "O5S: A Monte Carlo Code for Calculating Pulse Height Distributions Due to Monoenergetic Neutrons Incident on Organic Scintillators", ORNL-4160 (1968).
3) V. V. Verbinski et al., Nucl. Instr. and Methods, 65, 8 (1968).
4) J. A. Lockwood et al., Nucl. Instr. and Methods, 138, 353 (1976).
5) D. L. Smith, R. G. Polk and T. G. Miller, Nucl. Instr. and Methods, 64, 157 (1968).
6) R. Batchelor et al., Nucl. Instr. and Methods, 13, 70 (1961).
7) N. Sasamoto and S. Tanaka, Nucl. Instr. and Methods, 148, 395 (1978).
8) H. Hirayama and T. Nakamura, THIS MEMOIRS, 34, 188 (1972).
9) S. An et al., "Iron Shielding Benchmark Experiments at YAYOI", UTNL-R-0025, University of Tokyo (1975).
10) K. Shin et al., submitted to Nucl. Sci. and Eng.
11) K. Shin et al., Bull. Inst. Chem. Res., Kyoto Univ., 57, 102 (1979).
12) I. Langner, J. J. Schmidt and D. Wall, "Tables of Evaluated Nuclear Cross Sections for Reactor Materials", KFK-750, EUR-3715e EANDC(E)-88 "U", Kernforchungszentrum, Karlsruhe (1968).
13) S. K. Penny, W. E. Kinney and F. G. Perey, ENDF/B-III, material 1165, Brookhaven National Laboratory.
14) D. C. Irving, R. M. Freestone, Jr., and F. B. K. Kam, "OR5: A General-Purpose Monte Carlo

Neutron Transport Code", ORNL-3633 (1965).
15) M. W. McNaughton et al., Nucl. Instr. and Methods, 129, 241 (1975).
16) W. H. Barkas and M. J. Berger, "Tables of Energy Losses and Ranges of Heavy Charged Particles", NASA SP-3013 (1964).
17) H. Sugiyama, "Stopping Power and Range Tables for Heavy Ions", Circulars of the Electrotechnical Laboratory No. 181 (1974).
18) W. R. Burrus and V. V. Verbinski, Nucl. Instr. and Methods, 167, 181 (1969).
19) R. G. Soltsz, "Revised WANL ANISN Program User's Manual", WANL-TMI-1967 (1969).